ORGANIC CHEMISTRY

General method for iron-catalyzed multicomponent radical cascades–cross-couplings

Lei Liu[1]†, Maria Camila Aguilera[2]†, Wes Lee[1], Cassandra R. Youshaw[1], Michael L. Neidig[2]*, Osvaldo Gutierrez[1,3]*

Transition metal–catalyzed cross-coupling reactions are some of the most widely used methods in chemical synthesis. However, despite notable advantages of iron (Fe) as a potentially cheaper, more abundant, and less toxic transition metal catalyst, its practical application in multicomponent cross-couplings remains largely unsuccessful. We demonstrate 1,2-bis(dicyclohexylphosphino)ethane Fe–catalyzed coupling of α-boryl radicals (generated from selective radical addition to vinyl boronates) with Grignard reagents. Then, we extended the scope of these radical cascades by developing a general and broadly applicable Fe-catalyzed multicomponent annulation–cross-coupling protocol that engages a wide range of π-systems and permits the practical synthesis of cyclic fluorous compounds. Mechanistic studies are consistent with a bisarylated Fe(II) species being responsible for alkyl radical generation to initiate catalysis, while carbon-carbon bond formation proceeds between a monoarylated Fe(II) center and a transient alkyl radical.

Organoboron compounds are valuable and highly versatile reagents widely used in modern organic synthesis (*1*). In particular, the use of organoboron reagents in palladium-catalyzed Suzuki-Miyaura couplings is one of the top five most used reactions in drug discovery (*2*). Photoredox catalysis has further expanded the utility of alkyl organoboron compounds as versatile radical precursors for numerous transformations (*3*). More recently, vinyl organoboron reagents have been used as effective lynchpins in three-component nickel- and metallaphotoredox-catalyzed cross-coupling reactions, leading to alkyl boryl scaffolds primed for further functionalization (*4*–*9*). Despite these efforts, the equivalent iron (Fe)–catalyzed transformation remains highly desirable in pharmaceutical research because of Fe's low cost, abundance, and potential for distinct and complementary modes of reactivity.

Fe-catalyzed cross-couplings have enabled the union of diverse carbon (C)–centered radicals and organometallic partners (Fig. 1A). However, although organoboron reagents have found utility in Fe-catalyzed two-component cross-couplings (Suzuki-Miyaura), application in multicomponent cross-couplings remains an elusive transformation (Fig. 1B) (*10*–*15*). Here, we report the successful realization of Fe-catalyzed cross-coupling of α-boryl radicals (generated from selective radical addition to vinyl boronates) with Grignard reagents to form dicarbofunctionalized compounds (Fig. 1C). Furthermore, to address a long-standing challenge in multicomponent cross-couplings, we report a general Fe-catalyzed multicomponent annulation–cross-coupling (MAC) protocol that facilitates the practical synthesis of tetrafluoroethylene-containing carbocycles and derivatives, which were previously difficult to make (*16*). Last, spectroscopy experiments [in situ Mössbauer, electron paramagnetic resonance (EPR), and x-ray crystallography], density functional theory (DFT), and radical probes shed light on the mechanism of this transformation.

[1]Department of Chemistry and Biochemistry, University of Maryland, College Park, MD 20742, USA. [2]Department of Chemistry, University of Rochester, Rochester, NY 14627, USA. [3]Department of Chemistry, Texas A&M University, College Station, TX 77843, USA.
*Corresponding author. Email: og.labs@tamu.edu (O.G.); michael.neidig@rochester.edu (M.L.N.)
†These authors contributed equally to this work.

Development of a three-component coupling reaction

On the basis of our recently reported studies on Fe-catalyzed radical cross-couplings (*17*–*21*), we hypothesized that the electron-deficient nature of vinyl boronates and the rapid kinetics observed in the Fe-catalyzed Kumada cross-couplings could be coupled to engage transient α-boryl radicals in selective three-component radical cross-couplings (*22*–*24*). In this vein, we first tested the proposed three-component radical cross-coupling using a sterically hindered alkyl halide under the slow addition of aryl Grignard nucleophile to avoid competing two-component cross-coupling and biaryl formation. After extensive experimentation, we identified $FeCl_3$ (10 mol %) in combination with 1,2-bis(dicyclohexylphosphino)ethane **L1** (20 mol %) as an effective catalytic system that engages α-boryl radicals, presumably through regioselective Giese addition of *tert*-butyl radical to vinyl boronate **2a**, to form the desired product **4a** in 90% yield (tables S1 and S2). In contrast to existing nickel systems, the reaction proceeded in <1 hour at low temperatures. Precatalysts with weakly coordinating triflate or acetate groups diminished the efficiency of the system, whereas halides or acetylacetonate counterions had minor effect on the yields (table S2, entries 1 to 6). Furthermore, 1,2-bis(dicyclohexylphosphino)ethane **L1** was a distinctly effective ligand (table S2, entries 7 to 13). Control experiments demonstrated that both the ligand and Fe salt are crucial for the reaction to proceed (table S2, entries 17 to 19). Both alkyl iodides and bromides provided the desired product under these conditions (~90% yield), although diminished yields were observed with alkyl chlorides (table S2, entries 20 and 21).

Encouraged by these findings, we turned our attention to studying the generality of the three-component radical cascade transformation. As shown in Fig. 2, we observed a wide range of organomagnesium compounds to be suitable cross-coupling partners with alkyl α-boryl radicals. In particular, difunctionalization of vinyl boronates proceeded with good yields and excellent regioselectivity with mono- and disubstituted aryl Grignard nucleophiles that varied in electron density at the para- and meta positions (**4a** to **4q**) as well as (hetero)aryl nucleophiles (**4r**). Furthermore, in contrast to nickel and metallaphotoredox catalytic systems, this protocol is compatible with alkenyl and alkynyl nucleophiles, albeit with lower yields observed for the latter (**4s** to **4w**). However, ortho-substituted aryl Grignard reagents were less efficient, presumably because of increased steric demand (**4y**). Having established the reactivity with sp- and sp^2-hybridized Grignard nucleophiles, we next probed the alkyl halide scope (Fig. 2, bottom). A range of tertiary acyclic and cyclic aliphatic electrophiles afforded the desired products with good yields (**4a′** to **4f′**). Secondary alkyl halides (**4g′**) and tertiary alkyl halides bearing aryl or heteroatom substituents also formed the desired products (**4f′** and **4h′**). Last, we identified tertiary α-bromo esters as competent substrates, leading to **4i′** bearing both an ester and alkyl boron as versatile synthetic handles for further diversification. Despite substantial advances in the synthesis of organofluorinated compounds (*25*), selective and catalytic $C(sp^3)$–CF_2R bond formation remains challenging (*26*) and is exceedingly rare in Fe-catalyzed cross-couplings (*27*–*31*). Seeking to expand the alkyl radical scope, we investigated whether this protocol could provide direct access to versatile fluorinated alkyl boron compounds. As shown in Fig. 2, bottom, a wide range of fluoroalkyl radical precursors—including those containing alkyl, ester, silyl, heteroaryl, phenoxy, perfluoroalkyl, and protected aldehydes—proved compatible partners, which led to the desired 1,2-alkylfluorinated-aryl organoboron products (**4j′** to **4p′**) in good to excellent yield. The distinctive properties of C–F bonds (*32*–*35*), versatility of the alkyl boron bond, and practicality of this method are anticipated to provide rapid access to valuable fluoroalkyl boron building blocks for synthetic applications.

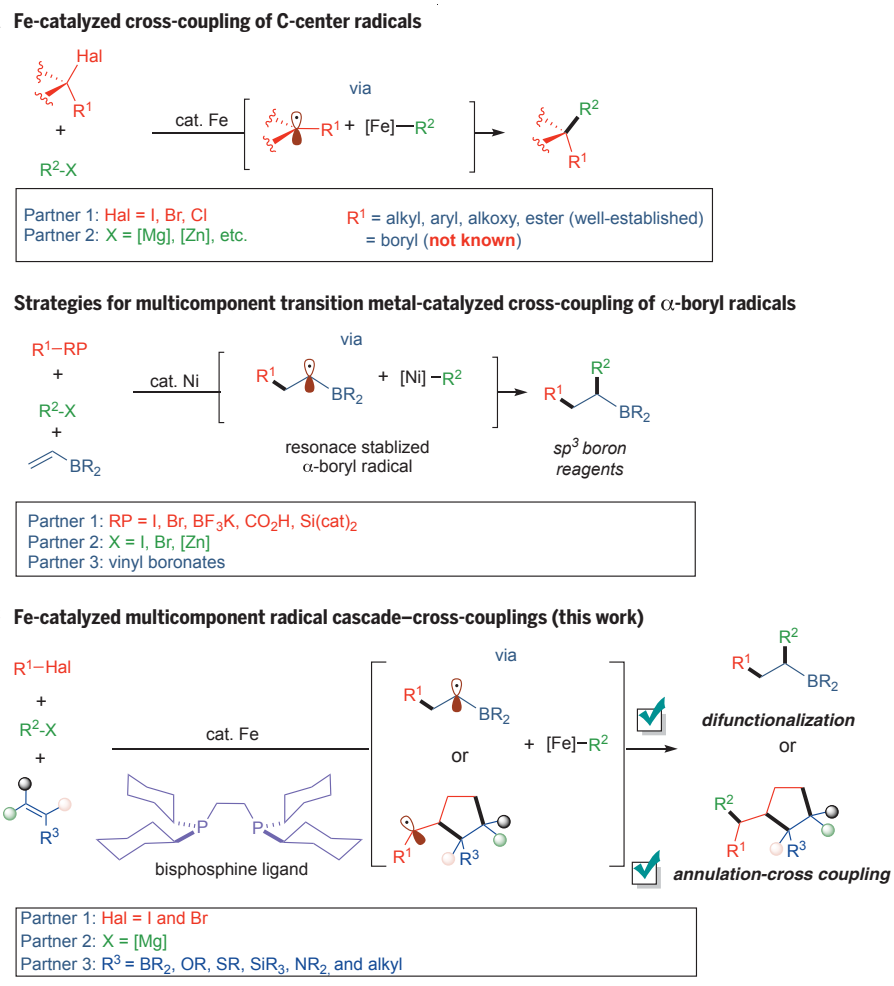

Fig. 1. Metal-catalyzed cross-coupling of α-boryl radicals. (**A**) Established methods for Fe-catalyzed C–C cross-coupling with alkyl radicals. (**B**) Current strategies for three-component trapping of α-boryl radicals. (**C**) Our report on the use of bisphosphine-iron complexes to promote radical cascade–cross-coupling reactions.

Extension to MACs

With the aim of expanding the applications of multicomponent radical cross-couplings, we turned our attention to alkyl halides with pendant alkenes as bifunctional coupling partners (*36*). Despite the utility of radical-based cyclization cascades and transition metal–catalyzed intramolecular cyclization-arylation in organic synthesis (*37*), the analogous intermolecular three-component radical cycloaddition-arylations have proven unexpectedly elusive. Furthermore, although incorporating CF_3, C_2F_5, and perfluoroalkyl alkyl groups in pharmaceutical research is common, practical and general synthetic methods for incorporation of the tetrafluoroethylene (-CF_2–CF_2-) moiety into cyclic compounds remains a challenge (*16*, *38*). We hypothesized that 4-bromo,3,3,4,4-tetrafluoro-1-butene **1s′,** which is commercially available and safe to handle, could serve as a general and practical lynchpin for the construction of tetrafluoroethylene-containing carbocycles that were previously hard to make. Similar conditions to those used for the three-component radical cross-coupling led to the MAC product **5a**, albeit in low yields because of competitive formation of dicarbofunctionalization product **4s′** (Fig. 3A). After screening of conditions, we found that by lowering the iron concentration and changing the catalyst-to-ligand ratio, we could shut down the dicarbofunctionalization pathway and increase yield of the annulation product **5a**. Presumably, lower catalyst concentration allows for more efficient 5-*exo* cyclization, leading to **int-2**, which in turn can undergo radical cross-coupling to form the annulation product (Fig. 3B).

With optimized conditions in hand, we next explored the generality with respect to alkene (Fig. 3C). Overall, a broad range of olefinic partners (**2a** to **zj**) (table S5) were found to be competent partners that lead to tetrafluoroethylene-containing drug-like scaffolds in one synthetic step. In particular, as shown in Fig. 3C, in addition to boron-substituted alkenes (**2a** and **2b**), vinyl silanes (**2c**), ketene acetals (**2d**), ethers (**2e** and **2v**), thioenols (**2f**), and enamines (**2g** and **2w**) were compatible. Furthermore, four-, five-, and six-membered (hetero)carbocycles bearing exo-cyclic alkenes (**2j** to **2r**) formed the corresponding spirocyclic compounds in good yields. We did not observe erosion of stereochemistry when using the enantiopure exo-methylene–containing pyrrolidine **2m** that led to the corresponding annulation-arylation product **5m**, as characterized by means of x-ray crystallography. In addition, this method allowed the gram-scale synthesis of spirocyclic compound **5p**, a derivative of sequosempervirin A (*39*), and fused bicyclic (hetero)cyclic structures, starting from the corresponding di- and trisubstituted cyclic (hetero)alkenes with good yields and modest to high regio- and diastereoselectivity (**2s** to **2x**). Acyclic olefins bearing alkyl chains with pendant functional groups—including aryl (**2z**), primary chloride (**2za**), alkene (**2zb**), alkyl boryl (**2zc**), unprotected alcohol (**2zd**) and amine (**2ze**), and alkyl ester (**2zf**)—were also competent partners. Tetrasubstituted alkenes and terminal alkynes also yielded the desired annulation-arylation products (**5zg**, **5zh**, **5zi**, and **5zj**), albeit in lower yields. To demonstrate potential for late-stage modification of bioactive compounds, we applied this protocol to natural products that bear alkene groups (**5zk** to **5zo**). We also explored the alkyl radical scope and found that other radical precursors could participate in the annulation (**5zp** to **5zu**).

We next explored the reaction scope of the nucleophile (Fig. 3D). In general, we found that para-substituted electron-rich and electron-poor aryl Grignard reagents formed the desired products (**5zv** to **5zza**). In addition, we found good yields across the board with aryl magnesium nucleophiles that bear electron-withdrawing groups (**5zza**, **5zzb**, **5zzf**, and **5zzg**); sterically hindered systems (**5zzc**, **5zzd, 5zze**, and **5zzi**), including those bearing C(sp^2)–Cl bonds for further functionalization; (hetero)aryls (**5zzk** and **5zzl**); and vinyl Grignard reagents (**5zzm** and **5zzn**).

Mechanistic studies

To elucidate the mechanism of this multicomponent iron-catalyzed cross-coupling, we used a combined spectroscopic, structural, computational, and organic synthetic approach. First, to provide direct insight into the iron intermediates involved in catalysis and enable the identification of the key iron species that initiates radical generation, we applied freeze-trapped 80 K ^{57}Fe Mössbauer and 10 K EPR spectroscopies, combined with single-crystal x-ray crystallography. For these spectroscopic studies, $^{57}FeBr_2$ was used as the starting Fe salt because it was a more accessible ^{57}Fe source, and it performed similarly to $FeCl_3$ under catalytic conditions. Two equivalents of **L1** (dcype) were

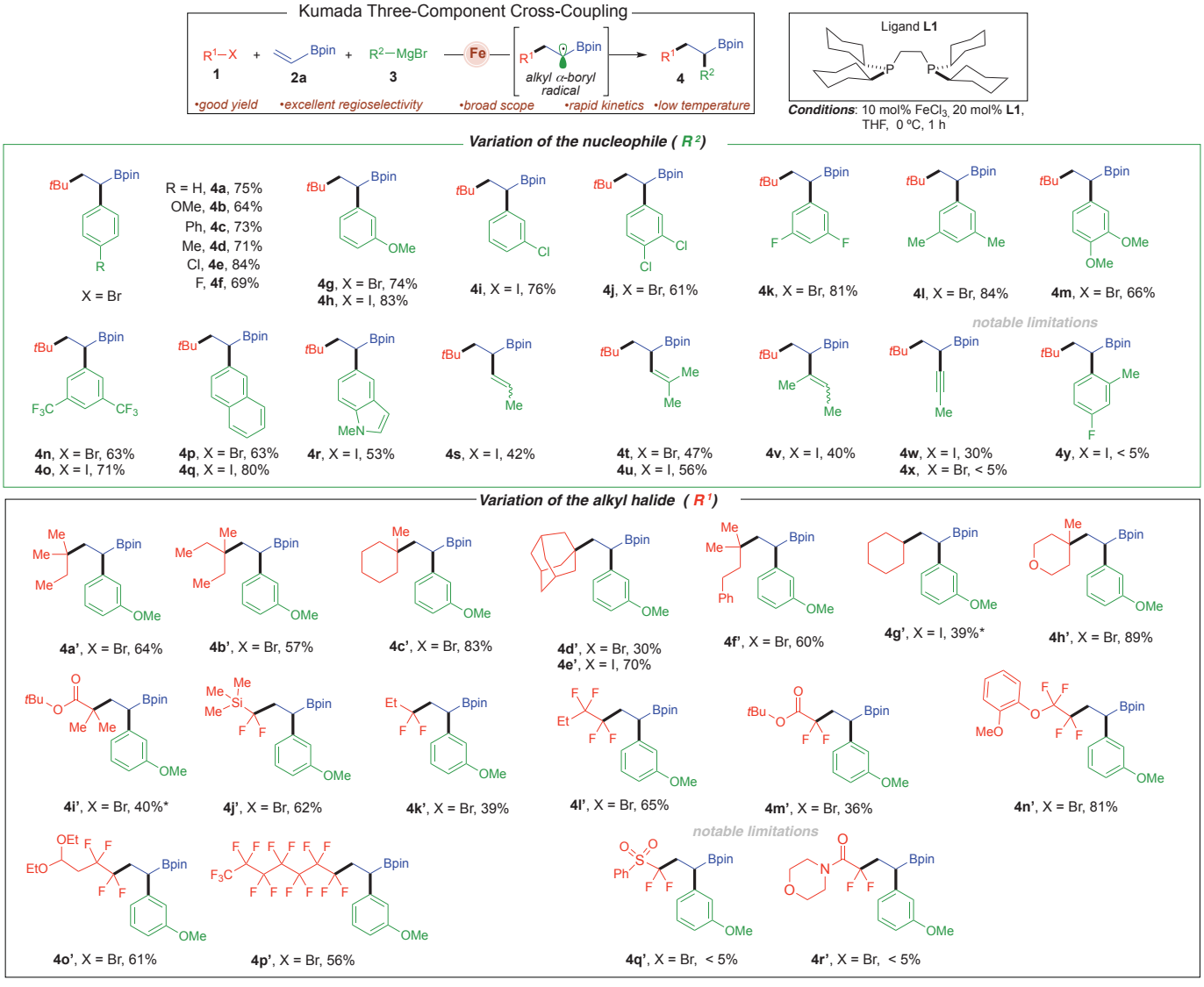

Fig. 2. Reaction scope of three-component dicarbofunctionalization of vinyl boronates by using bisphosphine-iron complexes as catalysts. Reactions were carried out on a 0.20-mmol scale at 0°C for 1 hour, performed with **1** (2.0 equiv), **2a** (1.0 equiv), Grignard reagent **3** (2.0 equiv) with THF (0.2 ml). Grignard reagent **3** was added dropwise by means of a syringe pump over 1 hour, isolated yield. *__1__ (5.0 equiv), Grignard **3** (5.5 equiv), and **3h**. Bpin, boronic acid pinacol ester; Me, methyl; Ph, phenyl; *t*Bu, *tert*-butyl.

combined with $^{57}FeBr_2$ in tetrahydrofuran (THF) for 10 min at 0°C, after which the solution was freeze-trapped in liquid N_2; an 80 K Mössbauer spectrum then revealed the formation of a single Fe species (δ = 0.72 mm/s and $|\Delta E_Q| = 3.21$ mm/s, where δ is the isomer shift and $|\Delta E_Q|$ is the quadrupole splitting) (table S6), which was later isolated and characterized by x-ray crystallography and Evans method nuclear magnetic resonance (NMR) as the high-spin Fe(II) dihalide complex Fe(dcype)Br_2 (**1**) [effective magnetic moment (μ_{eff}) = 5.2(1), δ = 0.73 mm/s, and $|\Delta E_Q| = 3.13$ mm/s for isolated material; numbers in parentheses indicate standard deviation] (Fig. 4A). The reaction of **1** with 1 equiv of the aryl Grignard reagent 3-methoxyphenyl magnesium bromide at 0°C resulted in the formation of a single Fe species with Mössbauer parameters of δ = 0.51 mm/s and $|\Delta E_Q| = 2.49$ mm/s, which is consistent with previously reported monoarylated Fe(II) bisphosphine complexes (Fig. 4A) (*40*, *41*). X-ray crystallography combined with Evans method NMR confirmed this species as the distorted tetrahedral, monoaryl high-spin Fe(II) complex Fe(dcype)BrAr (Ar, 3-$MeOC_6H_4$) [μ_{eff} = 5.0(2), δ = 0.52 mm/s, and $|\Delta E_Q| = 2.45$ mm/s for isolated material] (**2**).

Addition of a second equivalent of aryl Grignard reagent led to a color change of the solution from pale to brilliant yellow over the course of 1 min, which further evolved to dark green over 5 min. At that point, freeze-trapped Mössbauer spectroscopy indicated the formation of two new iron species, **3** and **4**, corresponding to 50 and 10% of the total Fe concentration, respectively (Fig. 4A). At a shorter reaction time (1 min), only 25% of species **2** had been converted to **3** without any formation of **4**. Further experiments revealed that species **4** could be accessed in higher amounts if excess aryl Grignard reagent is added (fig. S4A). This observation suggested the possible identity of **4** as a reduced Fe species, which was subsequently confirmed with x-ray crystallography to be (dcype)Fe{η^6-[3,3′-$(OMe)_2$-1,1′-$(C_6H_4)_2$]} (Fig. 4A and fig. S4B). The identification of this Fe(0) complex suggested that **3** was likely an Fe(II) bisaryl species formed before reductive elimination (δ = 0.23 mm/s and $|\Delta E_Q| =$ 4.35 mm/s). This assignment was subsequently

confirmed with crystallographic analysis as the bisarylated species Fe(dcype)Ar_2 (***3***), in which the large increase in the quadrupole splitting of ***3*** is consistent with the distorted square planar geometry of this Fe(II) complex. Although crystals of ***3*** repeatedly decayed over the course of the data collection, which limited the quality of the structure, the atomic assignments, overall geometry, connectivity, and identification of this complex are unambiguous. The product ***3*** was too thermally unstable for further characterization. However, literature precedent for S = 1 distorted square planar Fe phosphine compounds bearing two mesityl ligands, including their comparable Mössbauer parameters to ***3***, supports assignment of ***3*** as an intermediate-spin (S = 1) Fe(II) complex (*41*, *42*). This molecular geometry is atypical for bisaryl-Fe(II)-bisphosphines beyond mesityl complexes, which suggests an increased donor strength for **L1** that results from the cyclohexyl substituents. In addition, the identification of **4** indicates that ***3*** undergoes a two-electron reduction pathway similar to that previously observed in Fe(II)-SciOPP species (SciOPP, 1,2-{bis[3,5-di(*tert*-butyl)phenyl]phosphino}benzene) (*40*). Although all stoichiometric reactions were performed with an excess of **L1**, as prescribed for the catalytic reaction, all the iron species identified in situ contained only one bisphosphine per iron center.

We proceeded to evaluate the reactivity of the identified, transmetalated Fe(II)-aryl-bisphosphine species toward electrophile (2-iodo-2-methylpropane) to determine their potential for radical initiation in catalysis. Pseudo–single-turnover studies for the reaction of monoarylated species **2** (generated in situ) with an excess of 2-iodo-2-methylpropane (20 equiv) in the presence of vinyl boronic acid pinacol ester indicated that **2** is reactive toward electrophile at an observed rate (k_{obs}) of ~0.04 min^{-1} (figs. S5 and S6), which resulted in three-component product formation. However, the observed rate of reaction is far too slow to be catalytically relevant, including the initial radical generation, considering the average turnover frequency during catalysis (~0.17 min^{-1}). Conversely, Mössbauer spectroscopic studies indicated that ***3*** is highly reactive toward electrophile. The reaction of a mixture of **2** and ***3*** (generated in situ after 1 min) with excess 2-iodo-2-methylpropane (20 equiv) leads to the complete consumption of species ***3*** within 25 s with concomitant generation of complex **1**, whereas the complex **2** in solution does not react with electrophile, which is consistent with its aforementioned slow reactivity (Fig. 4B). However, when a similar reaction is performed in the presence of vinyl boronic acid pinacol ester, species **2** is also consumed (fig. S7), which suggests a likely recombination of the secondary radical (formed after addition of the tertiary radical to the alkene) with **2** to generate product (further insights are available in the supplementary materials, materials and methods). Although complex **4** was also found to be highly reactive toward excess electrophile (20 equiv) (fig. S8), only undesired side products, including the two-component coupling of the electrophile and alkene, were observed to form, which is consistent with the lack of the aryl component required to form the three-component product. Furthermore, the reaction of the bisarylated species ***3*** with electrophile is faster (<25 s) than its transformation to complex **4** (>1 min); thus, **4** is unlikely to be generated in any substantial amount under catalytic conditions, which is consistent with no observation of **4** during catalysis. However, formation of **4** is more facile when only 1 equiv of **L1** is used (fig. S9), providing one possible role of excess ligand in achieving optimal yields in catalysis, although other roles of the excess phosphine, such as coordination to magnesium cations, cannot be excluded (*43*). Overall, these reactivity studies identify the distorted square planar bisarylated Fe(II) complex ***3*** as the key iron species responsible for the initial radical formation with the alkyl electrophile, which is required as the first step to initiate catalysis. Details about the nature of C–C bond formation were studied by means of DFT calculations.

We bolstered these stoichiometric studies with in situ iron speciation studies during catalysis: 80 K Mössbauer and 10 K EPR spectroscopy experiments were carried out on freeze-trapped reaction samples at various time points throughout the catalytic reaction (10, 30, and 50 min) (fig. S10). The distribution of species during catalysis consisted of ~48% **1** and ~52% **2** by Mössbauer spectroscopy; no EPR active species were observed. The presence of **2** in such large quantities during catalysis is consistent with the previous observation that **2** reacts slowly with electrophile. Complex ***3*** being undetectable during catalysis is also consistent with the prior observation of its rapid reactivity toward electrophile.

We next considered the success of **L1** as the supporting ligand because other related bisphosphines resulted in substantially decreased product formation. To understand this effect, we compared the distribution of species formed under catalytically relevant conditions with tetraethyl ligand **L3**. The Mössbauer spectrum of the freeze-trapped solution after reaction of $^{57}FeBr_2$ with 2 equiv of **L3** [1,2-bis(diethylphosphino)ethane (depe)] at 0°C shows the formation of a single Fe species (δ = 0.47 mm/s and $|\Delta E_Q| = 1.51$ mm/s), which corresponds to the previously reported, distorted octahedral Fe(II) complex Fe(depe)$_2Br_2$ (***5***) (fig. S11) (*44*). Complex ***5*** also preferentially forms over the 1:1 **L3**:Fe complex, even when only 1 equiv of **L3** is used (fig. S12). Reaction of ***5*** with aryl Grignard (1 or 2 equiv) at 0°C led to a color change from brilliant yellow-green to orange within 5 min. Freeze-trapped Mössbauer spectroscopy indicated the formation of a single new Fe species **6** (δ = 0.30 mm/s and $|\Delta E_Q| = 0.27$ mm/s) (fig. S13), even at extended reaction times, with the reduced isomer shift (relative to complex ***5***) and small quadrupole splitting consistent with a distorted octahedral, arylated low-spin Fe(II) complex, as expected for the transmetalation of ***5*** with aryl Grignard reagent (*40*). Combined with additional reaction data at room temperature (fig. S13), this species is assigned to the monoarylated complex Fe(depe)$_2$BrAr. Reaction of **6** with 20 equiv of 2-iodo-2-methylpropane resulted in no consumption of this coordinatively saturated iron species, even at extended time points (20 min), which indicates limited or no reactivity toward electrophile (fig. S14). The observed slow transmetalation of ***5*** and lack of reactivity of **6** described above are consistent with their presence as the major Fe species in solution during catalysis (fig. S15). In the presence of excess nucleophile, a S = 1/2 Fe species could also be observed (fig. S16), which likely corresponds to a five-coordinate Fe(depe)$_2$X complex (X = Br or Ar), consistent with previously reported Fe(I) complexes formed as a result of the reaction of Fe-bisphosphines with aryl Grignard reagents (*44*, *45*). A coordinatively saturated, bisarylated Fe(depe)$_2Ar_2$ complex may also form in situ before reduction to Fe(I), although this species could not be unambiguously observed. The reduced Fe(I) species was found to be reactive toward electrophile in the presence of alkene (fig. S17), but the formation of only side products, including the two-component coupling of the electrophile and alkene, was observed, which is consistent with this Fe(I) species being unproductive for catalysis. Overall, these observations are consistent with the poor catalytic performance when using **L3** and highlight the importance of steric effects on the bisphosphine ligands in promoting the formation of coordinatively unsaturated Fe(II) species capable of initiating the radical formation as well as undergoing recombination to generate the desired product selectively.

Next, using vinyl cyclopropane as radical probe **2zp** (Fig. 5A), we observed the 1,5-dicarbofunctionalization product **4′** and no annulation product **5′** to be consistent with faster alkyl radical ring opening (k ~ 10^7 s^{-1}) than radical 5-*exo* cyclization (k ~ 10^5/s) and arylation (k ~ 10^4 s^{-1}) (*19*, *46*). In addition, consistent with the intermediacy of the alkyl radical, we also observed stereoconvergence in

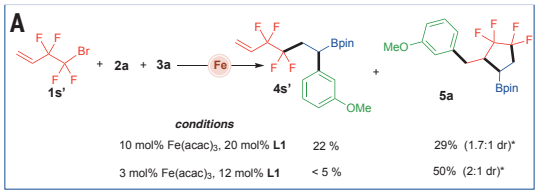

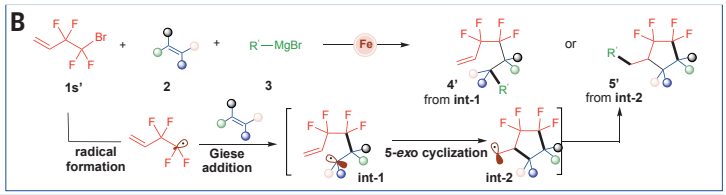

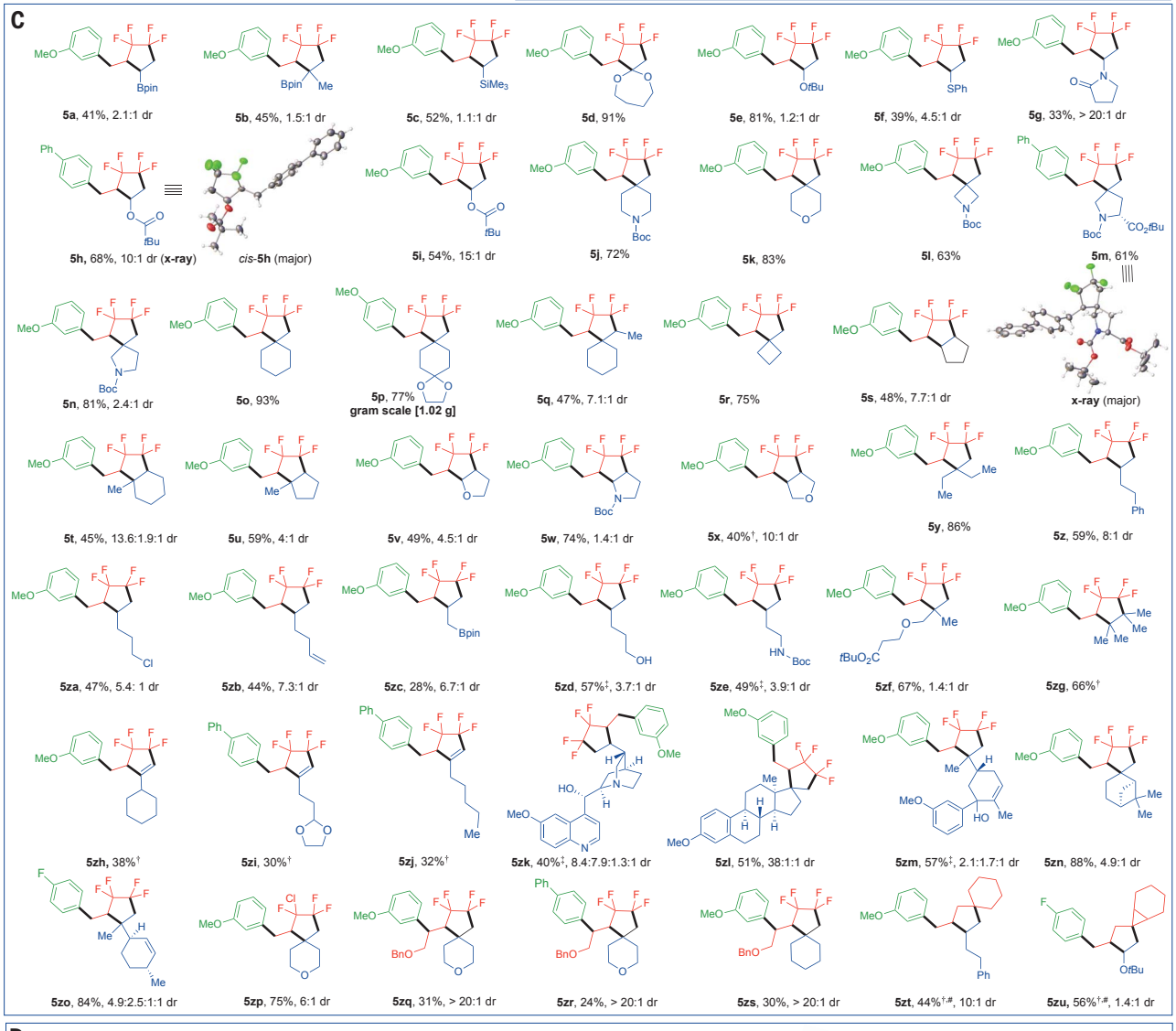

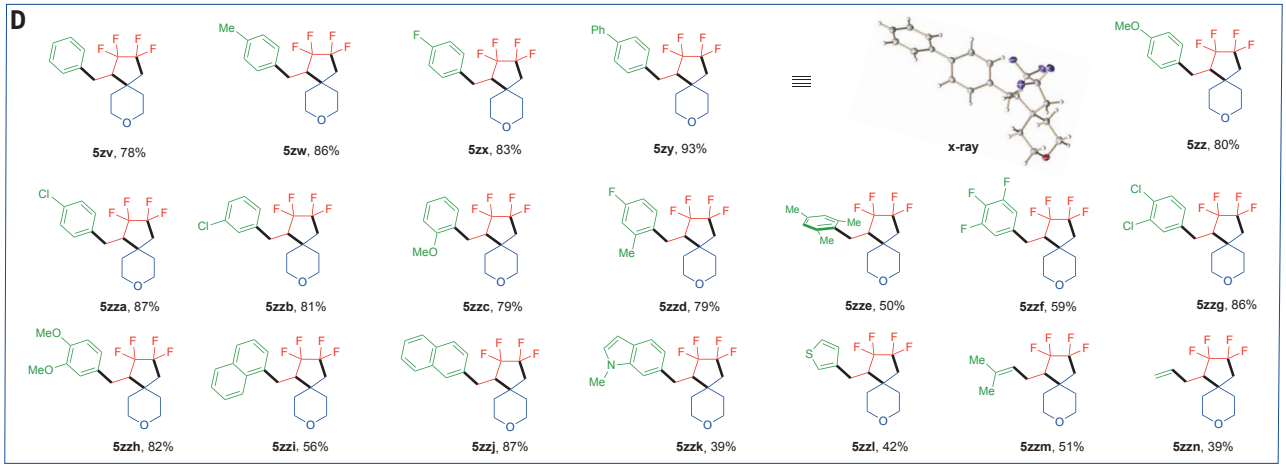

Fig. 3. Reaction scope of three-component annulation-arylation reaction sequence catalyzed by bisphosphine-iron catalysts. Reactions were carried out on a 0.20-mmol scale at 0°C for 1 hour, performed with **1** (1.0 equiv), **2** (1.5 equiv) Grignard reagent **3** (2.0 equiv), $Fe(acac)_3$ (3 mol %), and **L1** (12 mol %) with THF (0.2 ml). Grignard reagent **3** was added dropwise via a syringe pump over 1 hour. Reported yields and dr are from isolated yields. acac, acetylacetonate; Boc, *tert*-Butyloxycarbonyl; dr, diastereomeric ratio. *^{1}H NMR yield with CH_2Br_2 as internal standard. †Alkene or alkyne (14 equiv). ‡Grignard **3** (3.0 equiv). #No additional solvent.

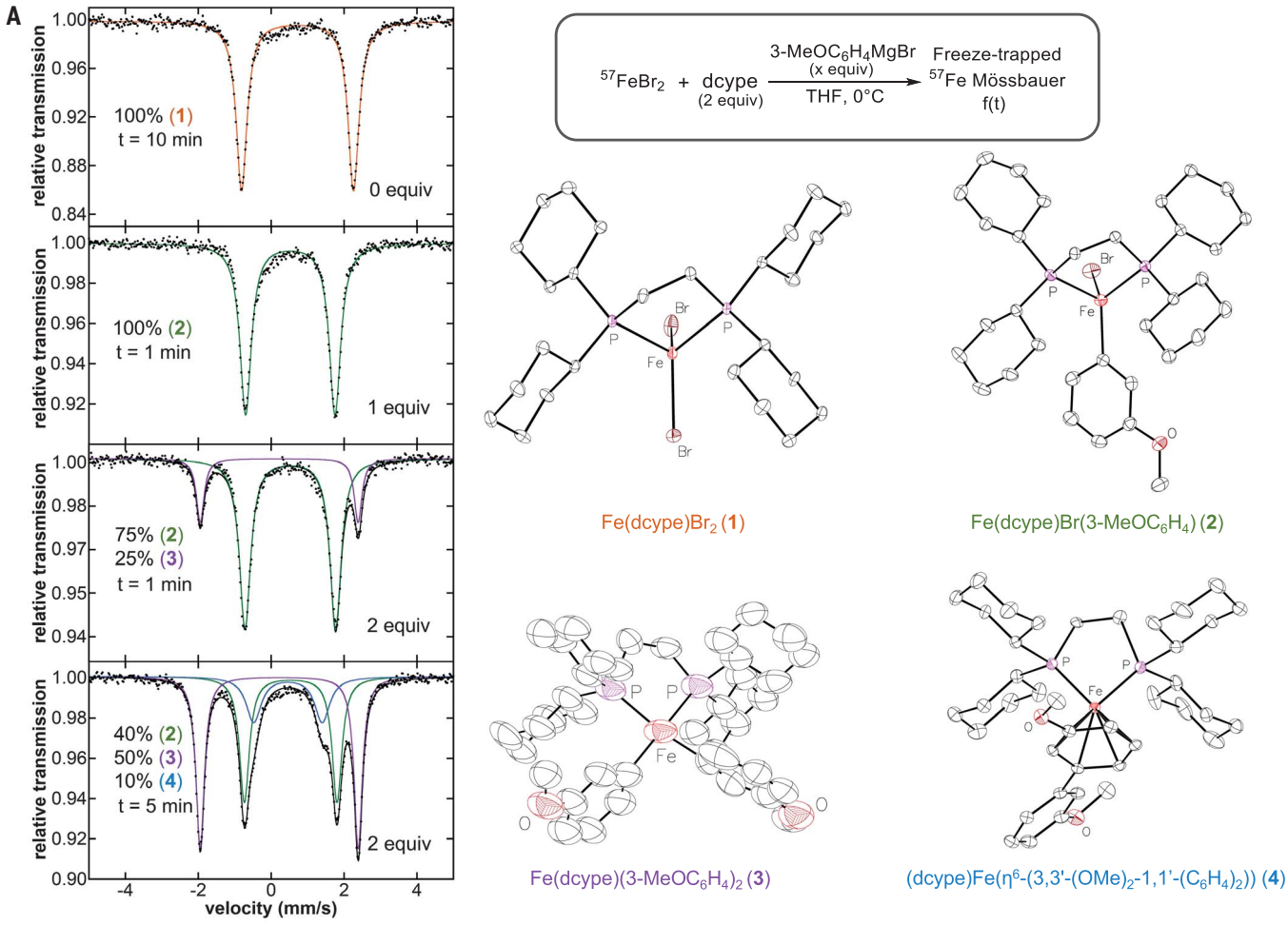

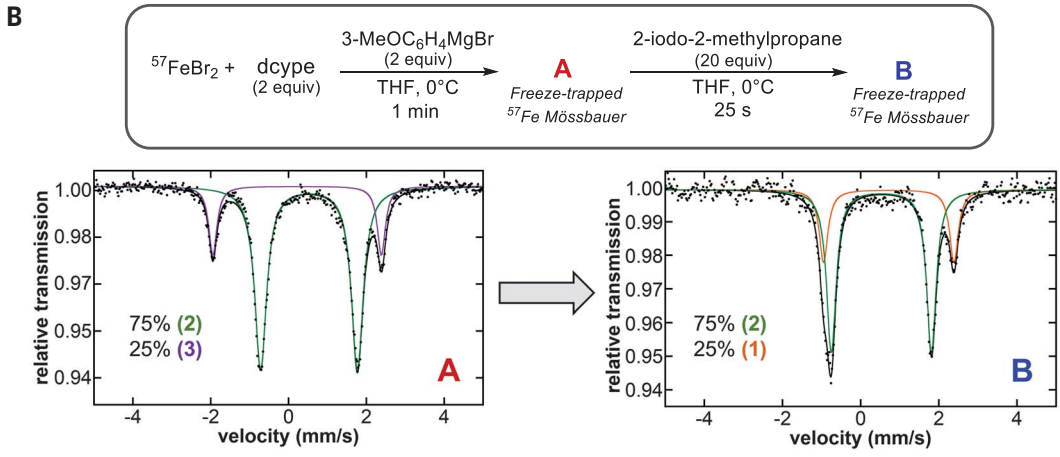

Fig. 4. Freeze-trapped 80 K Mössbauer spectra of stoichiometric reactions. (**A**) $^{57}FeBr_2$, 2 equiv of **L1**, and various equivalents of 3-$MeOC_6H_4MgBr$ (left). Combining SC-XRD and Mössbauer studies of crystalline material, the individual components were assigned as $Fe(dcype)Br_2$ (**1**) (orange), Fe(dcype)Br(3-$MeOC_4H_6$) (**2**) (green), $Fe(dcype)(3\text{-}MeOC_4H_6)_2$ (**3**) (purple), and (dcype)Fe{η^6-[3,3′-$(OMe)_2$-1,1′-$(C_4H_6)_2$]} (**4**) (blue). Thermal ellipsoids are shown at 50% probability. (**B**) The freeze-trapped 80 K Mössbauer spectrum of the in situ formed iron species upon reaction of $^{57}FeBr_2$ and 2 equiv of **L1**, with 2 equiv of 3-$MeOC_6H_4MgBr$ for 1 min (left) and following subsequent reaction with 2-iodo-2-methylpropane for 25 s (right).

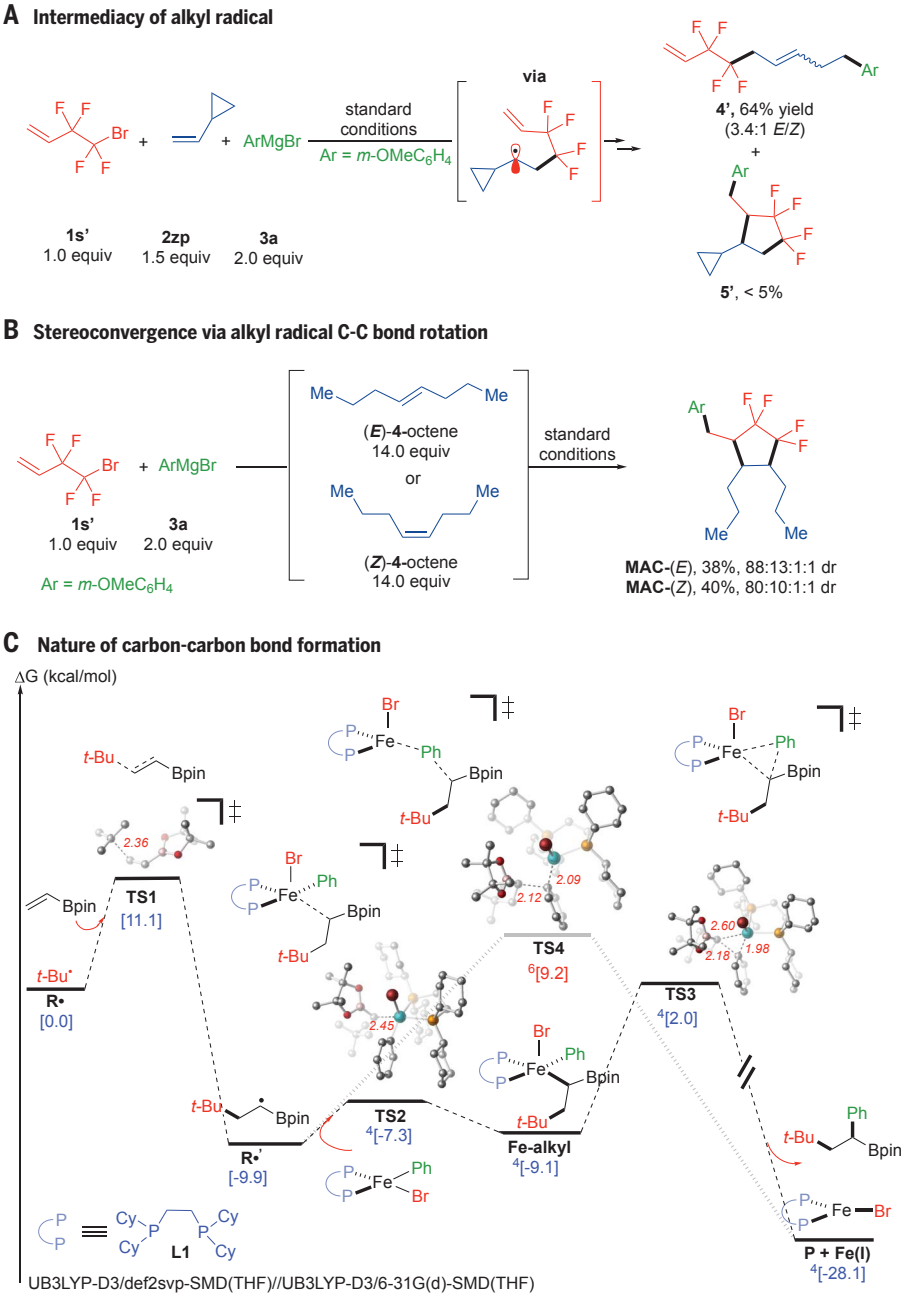

Fig. 5. Experimental and DFT calculations insights into the mechanism. (**A** and **B**) Standard conditions were carried out on a 0.20-mmol scale at 0°C; Grignard reagent **3a** was added dropwise by means of a syringe pump over 1 hour. Reported yields and dr are from isolated yields. (**C**) Computed lowest-energy pathway for the Fe-catalyzed multicomponent radical cascade cross-coupling reaction leading to dicarbofunctionalization of vinyl boronates. TS, transition state structure.

the three-component annulation, leading to the same product outcome by using either *E* or *Z* 4-octene, which suggests rapid equilibration (through sigma-bond rotation) before 5-*exo* radical cyclization-arylation (Fig. 5B). Last, to gain insight into the nature of the C–C bond formation, we turned to DFT calculations, which supported initial radical formation from an intermediate-spin distorted square planar bisarylated Fe(II) species through halogen abstraction (barrier, ~20 kcal/mol), which led to Fe(III) and tertiary radical (fig. S19). In turn, as shown in Fig. 5C, radical addition to vinyl boronate is predicted to be fast (barrier, ~11 kcal/mol) and irreversible, leading to α-boryl radical **R•'**. Then, this radical can rapidly and reversibly add (barrier, ~2.6 kcal/mol) to the corresponding high-spin distorted tetrahedral, monoarylated Fe(II) species, which leads to a distorted square pyramidal Fe(III)-alkyl intermediate. Subsequent irreversible reductive elimination by means of quartet spin state leads to the desired product and Fe(I) species, which can then restart the catalytic cycle (*17*, *47*). We also located the competing outer-sphere C–C forming transition state, but this pathway is less likely because of a much higher barrier (~19 kcal/mol) in comparison with the inner-sphere stepwise C–C bond formation (Fig. 5C, **TS4**). (Further mechanistic discussion and alternative pathways are provided in fig. S22.)

Overall, we anticipate that the method disclosed here will provide a practical and general route to functionalization of electron-rich and electron-deficient alkenes with various alkyl and hetero-substituents and application to late-stage functionalization of bioactive molecules.

REFERENCES AND NOTES

1. E. Fernández, A. Whiting, *Synthesis and Application of Organoboron Compounds* (Springer, 2015).
2. J. P. Wolfe, R. A. Singer, B. H. Yang, S. L. Buchwald, *J. Am. Chem. Soc.* **121**, 9550–9561 (1999).
3. J. C. Tellis, D. N. Primer, G. A. Molander, *Science* **345**, 433–436 (2014).
4. M. W. Campbell, J. S. Compton, C. B. Kelly, G. A. Molander, *J. Am. Chem. Soc.* **141**, 20069–20078 (2019).
5. A. García-Domínguez, R. Mondal, C. Nevado, *Angew. Chem. Int. Ed.* **58**, 12286–12290 (2019).
6. R. S. Mega, V. K. Duong, A. Noble, V. K. Aggarwal, *Angew. Chem. Int. Ed.* **59**, 4375–4379 (2020).
7. S.-Z. Sun, Y. Duan, R. S. Mega, R. J. Somerville, R. Martin, *Angew. Chem. Int. Ed.* **59**, 4370–4374 (2020).
8. M. Chierchia, P. Xu, G. J. Lovinger, J. P. Morken, *Angew. Chem. Int. Ed.* **58**, 14245–14249 (2019).
9. X.-X. Wang, X. Lu, S.-J. He, Y. Fu, *Chem. Sci.* **11**, 7950–7956 (2020).
10. T. Hatakeyama *et al.*, *J. Am. Chem. Soc.* **132**, 10674–10676 (2010).
11. H. M. O'Brien *et al.*, *Nat. Catal.* **1**, 429–437 (2018).
12. M. P. Crockett, A. S. Wong, B. Li, J. A. Byers, *Angew. Chem. Int. Ed.* **59**, 5392–5397 (2020).
13. R. B. Bedford *et al.*, *Organometallics* **33**, 5940–5943 (2014).
14. N. Kumar, R. R. Reddy, N. Eghbarieh, A. Masarwa, *Chem. Commun.* **56**, 13–25 (2020).
15. J. C. Lo *et al.*, *J. Am. Chem. Soc.* **139**, 2484–2503 (2017).
16. J. Václavík, I. Klímánková, A. Budinská, P. Beier, *Eur. J. Org. Chem.* **2018**, 3554–3593 (2018).
17. W. Lee, J. Zhou, O. Gutierrez, *J. Am. Chem. Soc.* **139**, 16126–16133 (2017).
18. L. Liu, W. Lee, M. Yuan, O. Gutierrez, *Comments Inorg. Chem.* **38**, 210–237 (2018).
19. L. Liu, W. Lee, J. Zhou, S. Bandyopadhyay, O. Gutierrez, *Tetrahedron* **75**, 129–136 (2019).
20. L. Liu *et al.*, *Chem. Sci.* **11**, 3146–3151 (2020).
21. L. Liu *et al.*, *Chem. Sci.* **11**, 8301–8305 (2020).
22. M. L. Neidig *et al.*, *Acc. Chem. Res.* **52**, 140–150 (2019).
23. J. D. Sears, P. G. N. Neate, M. L. Neidig, *J. Am. Chem. Soc.* **140**, 11872–11883 (2018).
24. D. G. Hall, Structure, properties, and preparation of boronic acid derivatives: in *Boronic acids* (Wiley, 2005), chap. 1, pp. 1–133.
25. M.-C. Belhomme, T. Besset, T. Poisson, X. Pannecoucke, *Chemistry* **21**, 12836–12865 (2015).
26. L. An, C. Xu, X. Zhang, *Nat. Commun.* **8**, 1460 (2017).
27. L. An, Y.-L. Xiao, S. Zhang, X. Zhang, *Angew. Chem. Int. Ed.* **57**, 6921–6925 (2018).
28. X. X. Rong, H.-Q. Pan, W. R. Dolbier Jr., B. E. Smart, *J. Am. Chem. Soc.* **116**, 4521–4522 (1994).
29. J. Derosa, O. Apolinar, T. Kang, V. T. Tran, K. M. Engle, *Chem. Sci.* **11**, 4287–4296 (2020).
30. D. V. Avila *et al.*, *J. Am. Chem. Soc.* **116**, 99–104 (1994).
31. X. Lin, F. Zheng, F.-L. Qing, *Organometallics* **31**, 1578–1582 (2012).
32. D. O'Hagan, *Chem. Soc. Rev.* **37**, 308–319 (2008).
33. K. Müller, C. Faeh, F. Diederich, *Science* **317**, 1881–1886 (2007).
34. S. Purser, P. R. Moore, S. Swallow, V. Gouverneur, *Chem. Soc. Rev.* **37**, 320–330 (2008).

35. M. A. Miller, E. M. Sletten, *ChemBioChem* **21**, 3451–3462 (2020).
36. J. Boström, D. G. Brown, R. J. Young, G. M. Keserü, *Nat. Rev. Drug Discov.* **17**, 709–727 (2018).
37. A. Studer, D. P. Curran, *Angew. Chem. Int. Ed.* **55**, 58–102 (2016).
38. L. Li *et al*., *Angew. Chem. Int. Ed.* **56**, 9971–9975 (2017).
39. S. Maity, S. Ghosh, *Tetrahedron Lett.* **48**, 3355–3358 (2007).
40. S. L. Daifuku, J. L. Kneebone, B. E. R. Snyder, M. L. Neidig, *J. Am. Chem. Soc.* **137**, 11432–11444 (2015).
41. S. L. Daifuku, M. H. Al-Afyouni, B. E. R. Snyder, J. L. Kneebone, M. L. Neidig, *J. Am. Chem. Soc.* **136**, 9132–9143 (2014).
42. E. J. Hawrelak *et al*., *Inorg. Chem.* **44**, 3103–3111 (2005).
43. A. M. Messinis *et al*., *Nat. Catal.* **2**, 123–133 (2019).
44. D. J. Evans, R. A. Henderson, A. Hills, D. L. Hughes, K. E. Oglieve, *J. Chem. Soc., Dalton Trans.* (7): 1259–1265 (1992).
45. R. B. Bedford *et al*., *Organometallics* **33**, 5767–5780 (2014).
46. M. Newcomb, in *Encyclopedia of Radicals in Chemistry, Biology and Materials*, C. Chatgilialoglu and A. Studer, Eds. (Wiley, 2012).
47. A. K. Sharma *et al*., *J. Am. Chem. Soc.* **139**, 16117–16125 (2017).

ACKNOWLEDGMENTS

We thank P. Y. Zavalij (University of Maryland) and W. W. Brennessel (University of Rochester) for help with x-ray diffraction and Y. Li (University of Maryland) for help with the high-resolution mass spectrometry. **Funding:** Funding was provided by the National Institutes of Health (grant R35GM137797 to O.G. and R01GM111480 to M.L.N.) and the National Science Foundation (CAREER 1751568 to O.G.). **Author contributions:** L.L. developed the method and performed DFT calculations, and M.C.A. carried out the mechanistic studies. W.L. carried out DFT calculations and chromatography. C.R.Y. performed materials preparation and chromatography. O.G. and M.L.N. directed the investigations and wrote the manuscript with revisions provided by the other authors. **Competing interests:** The authors declare that they have no competing interests. **Data and materials availability:** Crystallographic data are available free of charge from the Cambridge Crystallographic Data Center under reference nos. CCDC-2085294, CCDC-2085295, CCDC-2085297, CCDC-2085565, CCDC-2085566, CCDC-2085567, and CCDC-2085568. All other data are available in the main text or the supplementary materials.

SUPPLEMENTARY MATERIALS

science.org/doi/10.1126/science.abj6005
Materials and Methods
Supplementary Text
Figs. S1 to S22
Tables S1 to S13
References (*48*–*69*)

24 May 2021; accepted 9 August 2021
10.1126/science.abj6005

Science

General method for iron-catalyzed multicomponent radical cascades–cross-couplings

Lei LiuMaria Camila AguileraWes LeeCassandra R. YoushawMichael L. NeidigOsvaldo Gutierrez

Science, 374 (6566), • DOI: 10.1126/science.abj6005

Iron links a trio

Iron holds particular appeal as a catalytic metal—it is safe and abundant, as well as a mainstay of enzymatic reactivity. Nonetheless, in synthetic construction of carbon-carbon bonds, modern chemists have largely had to rely on rarer metals such as palladium. Liu *et al*. now report that coordination of iron by a bulky chelating phosphine ligand enables efficient mutual coupling of three different reactants—an alkyl halide, an aryl Grignard, and an olefin—to form two carbon-carbon bonds (see the Perspective by Lefèvre). A combination of Mössbauer spectroscopy, crystallography, and computational simulations illuminates the mechanism. —JSY

Science (ISSN) is published by the American Association for the Advancement of Science. 1200 New York Avenue NW, Washington, DC 20005. The title *Science* is a registered trademark of AAAS.